Photoluminescence intensity of single wall carbon nanotubes

Y. Oyama[a], R. Saito[*a], K. Sato[a], J. Jiang[a], Ge. G. Samsonidze[e], A. Grüneis[b],

Y. Miyauchi[c], S. Maruyama[c], A. Jorio[d,f], G. Dresselhaus[g], and M. S. Dresselhaus[e,f]

[a]Department of Physics, Tohoku University and CREST, Sendai, 980-8578, Japan

[b]Institute for Solid State Research, Leibnitz Institute for Solid

State and Materials Research, 01171 Dresden, Germany

[c]Department of Mechanical Engineering,

The University of Tokyo, 7-3-1 Hongo,

Bunkyo-ku, Tokyo 113-8656, Japan

[d]Departamento de Física, Universidade Federal de Minas Gerais,

Belo Horizonte - MG, 30123-970 Brazil and

[e]Department of Electrical Engineering and Computer Science,

[f]Department of Physics, [g]Francis Bitter Magnet Laboratory,

Massachusetts Institute of Technology, Cambridge, MA 02139-4307

(Dated: September 15, 2005)

Abstract

The photoluminescence (PL) intensity of a single wall carbon nanotube (SWNT) is calculated for each (n, m) by multiplying the photon-absorption, relaxation and photon-emission matrix elements. The intensity depends on chirality and "type I vs type II" for smaller diameter semiconducting SWNTs (less than 1 nm). By comparing the calculated results with the experimental PL intensity of SWNTs prepared by chemical vapor deposition at different temperatures, we find that the abundance of (n, m) nanotubes with smaller diameters should exhibit a strong chirality dependence, which may be related to the stability of their caps.

* Corresponding Author: rsaito@phys.tohoku.ac.jp fax:+81-22-795-6447

1. INTRODUCTION

Recently, photoluminescence (PL) spectroscopy for semiconducting single wall carbon nanotubes (SWNTs) which are wrapped by surfactants or freely suspended in the air has been investigated for possible optical device applications in the infrared region [1–5]. A strong PL emission peak is seen for an (n, m) nanotube at the energy E_{11}^S when excited by a strong absorption at E_{22}^S, where E_{ii}^S is the energy separation between van Hove singularities for the ground and excited states. The energy separation can be understood in terms of one-electron energy bands, given by an extended tight-binding calculation with structure optimization[6] and exciton formation in the presence of an electron-electron interaction which together are known as the many body effect[6, 7].

When we plot the excitation energy as a function of PL energy, each (n, m) peak intensity shows a strong chirality dependence. This dependence comes from: (1) the abundance of (n, m) nanotubes synthesized by some method and (2) the intrinsic PL intensity depending on (n, m). In this paper we calculate the PL intensity as a function of (n, m) and we try to obtain the abundance of each (n, m) species obtained by the alcohol catalytic chemical vapor deposition (ACCVD) method with different synthesis temperatures. We show that the diameter distribution of CVD SWNTs gives an asymmetric shape around the most abundant (n, m) peak and especially for smaller diameter nanotubes, the abundance has no regular chirality dependence.

In PL, we expect (1) an induced absorption of light at E_{22}^S, (2) relaxation from E_{22}^S to E_{11}^S by an electron-phonon interaction, and (3) spontaneous emission at E_{11}^S. The PL intensity is expressed by the product of these three factors. Here we assume in accordance with how the experiments are typically performed that (a) the photon absorption and emission is continuous in time, (b) the excitation power of the light is not so strong and therefore no saturation of the absorption is expected, (c) the electron-photon interaction is sufficiently slow compared with the electron-phonon interaction[8, 9] and that (d) the initial fast relaxation by the electron-electron interaction does not affect the PL intensity. The last assumption is justified for the case that the excitation energy is close to E_{22}^S.

When we consider the relaxation path from E_{22}^S to E_{11}^S in a SWNT, we can expect many different kinds of paths by emitting and absorbing many phonons with different phonon modes which satisfy energy-momentum conservation. Thus it is very hard to obtain an

averaged relaxation rate for an exciton transition from E_{22}^S to E_{11}^S. Here we simply assume that the relaxation rate of the transition from the energy minimum of the E_{22}^S band to the E_{11}^S energy band and to the other E_{22}^S band states by absorbing one phonon is a rate representative of the whole process. This rate may determine the total flow of electrons to E_{11}^S.

In section 2, we show how to calculate the photon absorption and emission and the electron-phonon interaction in SWNTs. In section 3, we compare the calculated results for the PL intensity with experimental results obtained from samples prepared by the high pressure CO method (HiPCO) and from ACCVD samples prepared at different temperatures. In section 4, a summary of this paper is given.

2. MATRIX ELEMENT CALCULATION

A. Photon absorption and emission

The calculation of the photon-absorption and emission matrix element is based on our previous paper.[10] However, we have since then added some factors to give the relative intensity per unit length of a SWNT within a relaxation time. Thus we again give the formula that is also used in the present calculation. The optical transition matrix element $\langle f|H_{\mathrm{opt}}|i\rangle$ is generally expressed within the dipole approximation, $\exp(i\mathbf{k}\cdot\mathbf{r})\simeq 1$, as

$$
\begin{aligned}
\langle f|H_{\mathrm{opt}}|i\rangle \;=\; &-i\frac{e\hbar}{m}\sqrt{\frac{\hbar}{2\epsilon_0 V}}\sum_{\mathbf{k}\lambda}\frac{1}{\sqrt{\omega_{\mathbf{k}\lambda}}}\langle\Psi_f|\mathbf{P}_{\mathbf{k}\lambda}\cdot\nabla|\Psi_i\rangle \\
&\times
\begin{cases}
\sqrt{n_{\mathbf{k}\lambda}}\;e^{i(\omega_{fi}-\omega)t} & \text{(absorption)} \\[2mm]
\sqrt{n_{\mathbf{k}\lambda}+1}\;e^{i(\omega_{fi}+\omega)t} & \text{(emission)},
\end{cases}
\end{aligned}
\tag{1}
$$

in which $\mathbf{P}_{\mathbf{k}\lambda}$, $n_{\mathbf{k}\lambda}$ and $\omega_{\mathbf{k}\lambda}$ are the polarization vector, the number and the frequency of photons with wavevector $\mathbf{k}$ and mode λ, respectively. Here ω_{fi} is the energy separation in frequency between the initial and final states.

The transition rate as a function of time from the initial state to the final state, $W_{fi}(t)$,

is given as a function of time by Fermi's golden rule

$$
\begin{aligned}
W_{fi}(t) &= \frac{1}{t\hbar^2}\left|\int_0^t \langle f|H_{\text{opt}}|i\rangle dt'\right|^2 \\
&= \frac{1}{t\hbar^2}\left(\frac{e\hbar}{m}\right)^2\frac{\hbar}{2\epsilon_0 V\omega}|\langle\Psi_f|\mathbf{P}\cdot\nabla|\Psi_i\rangle|^2 \\
&\times \begin{cases} n_{\mathbf{k}\lambda}\dfrac{4\sin^2[(\omega_{fi}-\omega)t/2]}{(\omega_{fi}-\omega)^2} & \text{(absorption)} \\ (n_{\mathbf{k}\lambda}+1)\dfrac{4\sin^2[(\omega_{fi}+\omega)t/2]}{(\omega_{fi}+\omega)^2} & \text{(emission)}. \end{cases}
\end{aligned}
\tag{2}
$$

The unity in $n_{\mathbf{k}\lambda}+1$ for emission corresponds to the spontaneous emission of light, while the term proportional to $n_{\mathbf{k}\lambda}$ corresponds to the induced emission (or absorption).

In the case of the spontaneous emission, the density of final states is given by

$$
\rho_{\mathbf{k}}d\mathbf{k} = \left(\frac{L}{2\pi}\right)^3 4\pi k^2 dk = \frac{V}{2\pi^2 c^3}\omega^2 d\omega,
\tag{3}
$$

where we take only the polarization direction of the light parallel to the nanotube axis[11].

When we integrate the terms corresponding to the spontaneous emission over ω, we can take ρ_ω and $|\langle\Psi_f|\mathbf{P}\cdot\nabla|\Psi_i\rangle|^2$ out of the integrand around $\omega \simeq \omega_{if}$ and we then get

$$
W_{\text{em}} = \frac{e^2\hbar\omega_{if}}{2\pi\epsilon_0 m^2 c^3}|\langle\Psi_f|\mathbf{P}\cdot\nabla|\Psi_i\rangle|^2.
\tag{4}
$$

The intensity of the spontaneous emission is proportional to the photon energy ω_{if}. On the other hand, the intensity of the induced absorption can be calculated by replacing $n_{\mathbf{k}\lambda}$ by $VI(\omega)d\omega/c\hbar\omega\gamma$,[12] then

$$
W_{\text{ab}} = \frac{\pi e^2 I}{\epsilon_0\gamma cm^2\omega_{fi}^2}|\langle\Psi_f|\mathbf{P}\cdot\nabla|\Psi_i\rangle|^2,
\tag{5}
$$

where I is the intensity of the incident light and γ is the spectral linewidth in units of $[1/s]$.

B. Electron-phonon interaction

The electron-phonon interaction is calculated from the deformation potential of the lattice,

$$
\langle f|H_{\text{e-ph}}|i\rangle = \langle\Psi_f(\mathbf{r},\mathbf{k}',t)|\delta V(\mathbf{r},\mathbf{q},t)|\Psi_i(\mathbf{r},\mathbf{k},t)\rangle.
\tag{6}
$$

The deformation potential vectors are calculated by the extended tight-binding potential and wavefunction using the inter-atomic potentials proposed by Porezag[13].

4

It is noted that we properly considered the effect on the deformation potential of the curvature effect and the on-site energy term[14]. Details of the method will be reported elsewhere. The scattering probability from $\mathbf{k}$ to all possible $\mathbf{k}'$ by the νth phonon mode is given by

$$
\begin{aligned}
W_{\mathbf{k}}^{\nu} &= \frac{S}{8\pi M d_t} \sum_{\mu',k'} \frac{|D_{\nu}(\mathbf{k},\mathbf{k}')|^2}{\omega_{\nu}(\mathbf{k}'-\mathbf{k})} \left[\frac{dE(\mu',k')}{dk'}\right]^{-1} \\
&\times \left\{ \frac{\delta(\omega(\mathbf{k}')-\omega(\mathbf{k})-\omega_{\nu}(\mathbf{k}'-\mathbf{k}))}{e^{\beta\hbar\omega_{\nu}(\mathbf{k}'-\mathbf{k})}-1} \right. \\
&\left. + \frac{\delta(\omega(\mathbf{k}')-\omega(\mathbf{k})+\omega_{\nu}(\mathbf{k}'-\mathbf{k}))}{1-e^{-\beta\hbar\omega_{\nu}(\mathbf{k}'-\mathbf{k})}} \right\},
\end{aligned}
\tag{7}
$$

where D_{ν} is the electron-phonon matrix element, $S = \sqrt{3}a^2/2$ is the area of a 2D graphite unit cell, d_t is the nanotube diameter, and M is the carbon atom mass[15]. The second and third lines on the right-hand side of Eq.(7) describe the phonon absorption and emission processes, respectively. The summation in Eq.(7) is over a series of points on cutting lines that satisfy both energy and momentum conservation. Using Eq.(7), we can get the relaxation time for each phonon mode as well as the total relaxation time[9].

3. CALCULATED RESULTS

A. Induced absorption and spontaneous emission

First we calculate the probability of induced absorption and spontaneous emission of an (n,m) SWNT, at the E_{22}^S and E_{11}^S excitation energies, respectively. In a one-dimensional material such as a SWNT, electron-electron and exciton effects should be included for obtaining the excitation and emission energies[16–18]. In our previous calculation, these two effects were found to be large and to mostly cancel each other. The final correction to the one-electron energy is on the order of 0.1eV and this can be expressed as a function of diameter and chiral angle[7]. Here we simply use E_{22}^S and E_{11}^S values as the one-electron energies obtained by the extended tight-binding calculation[7] and by including the many body correction term to this calculation[6]. For simplicity, we did not here consider the effect of the localized wavefunction of an exciton. We still need to investigate the form of the wavefunction of the photo-excited exciton and its relaxation by emitting a phonon, which will be a future work. Recently some of the present authors published a paper[19] showing that a Raman analysis and an optical absorption analysis of the same sample give
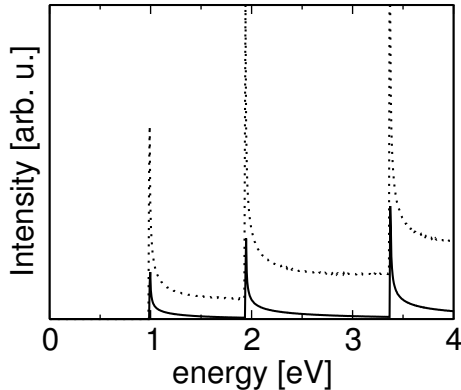
5

FIG. 1: Calculated photon absorption spectra for a (6,5) SWNT (solid line). The joint density of states (JDOS) is shown for comparison (dotted line).

the same result, which indicates that the process near E_{22}^S is more important for explaining the chirality dependence than the process near E_{11}^S.

The transition probability is expressed by the product of $M_{\text{opt}} = |\mathbf{P} \cdot \langle \Psi_f | \nabla | \Psi_i \rangle|^2$ and the joint density of states (JDOS). In Fig. 1 we plot the JDOS for a (6,5) SWNT in units of states/eV/(carbon atom), (dotted line) and the product of the JDOS and M_{opt} for polarization parallel to the nanotube axis (solid line), respectively. Because of selection rules, the matrix element has a maximum value around the E_{ii}^S positions, which results in a sharp photon absorption around the E_{ii}^S point, even though there is a continuous JDOS value as a function of energy.

In Fig. 2, we show the (a) induced absorption intensity at $E_{22}^S \pm 0.05$eV and the (b) spontaneous emission intensity at $E_{11}^S \pm 0.05$eV for semiconducting (n, m) SWNTs whose diameters lies in the range 0.6 nm $< d_t <$ 1.5 nm. Open and solid dots denote type I and II semiconducting SWNTs, respectively, in which the values of mod $(2n + m, 3)$ are 1 and 2, respectively[6]. We connect dots with the same $2n + m$ values to show both the family pattern and the chiral angle dependence. The integration width 0.05eV is taken from the experiment[5] where the JDOS does not show an ideal peak but rather shows some width around 0.05eV. As we can see from Fig. 2(a), the induced absorption has a linear dependence on diameter which is known from Eq. (5). The absorption intensity for type I semiconducting tubes is stronger than that for type II tubes over this wide diameter region. The reason why the intensity for type I is stronger than for type II is that the matrix element as a function of k is highly anisotropic around the K point[10], and thus the matrix element for
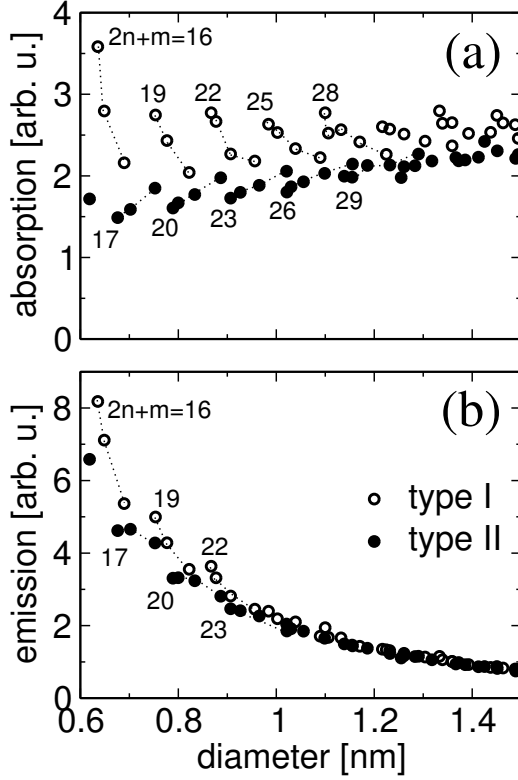
6

FIG. 2: (a) Induced absorption intensity at $E_{22}^S \pm 0.05$ eV as a function of diameter. Open and solid dots denote type I and II semiconducting SWNTs, respectively. (b) Spontaneous emission intensity at $E_{11}^S \pm 0.05$ eV which is inversely proportional to the square of the tube diameter. Points with the same indicated $2n + m$ values are connected.

semiconducting type I SWNTs, which have their vHS k in the direction of $K - M$, becomes larger. The singularity in the JDOS for type II semiconducting SWNTs is more singular than for type I tubes because of the effect of trigonal warping on the equi-energy contour[20]. The touching of the cutting line to the equi-energy contour is longer for type II SWNTs than for type I SWNTs and this effect gives rise to a larger JDOS value. Nevertheless the total intensity is mainly determined by the matrix element. The large (the small) values for type I (II) correspond to near zigzag SWNTs ($\theta \sim 0°$) and the central intensities for type I and II tubes correspond to near armchair SWNTs ($\theta \sim 30°$).

On the other hand, the spontaneous emission intensity is inversely proportional to the square of the tube diameter, as shown in Fig. 2(b), which can be understood by Eq. (4). Compared with the induced absorption, the difference between the predicted spontaneous emission for type I and II semiconducting tubes is small.

7

For a given diameter SWNT, the induced absorption intensity W_{ab} and the spontaneous emission intensity W_{em} are expressed, respectively, by $W_{\mathrm{ab}} = M/E_{22}^2$ and $W_{\mathrm{em}} = M \times E_{11}$, which are given by Eqs. (5) and (4), respectively. Since we know from Fig. 2 that $E_{22}^{\mathrm{I}} < E_{22}^{\mathrm{II}}$ and $M^{\mathrm{I}} > M^{\mathrm{II}}$, we get $W_{\mathrm{ab}}^{\mathrm{I}} = M^{\mathrm{I}}/(E_{22}^{\mathrm{I}})^2 > W_{\mathrm{ab}}^{\mathrm{II}} = M^{\mathrm{II}}/(E_{22}^{\mathrm{II}})^2$. As for W_{em}, since the two inequalities of $E_{11}^{\mathrm{I}} > E_{11}^{\mathrm{II}}$ and $M^{\mathrm{I}} < M^{\mathrm{II}}$ nearly cancel each other, thus we get $W_{\mathrm{em}}^{\mathrm{I}} = M^{\mathrm{I}} \times E_{11}^{\mathrm{I}} > W_{\mathrm{em}}^{\mathrm{II}} = M^{\mathrm{II}} \times E_{11}^{\mathrm{II}}$. Thus the chirality dependence of the relative absorption and emission intensities is understood on the basis of the trigonal warping effect.

B. Relaxation process by phonons

The PL intensity is expected to be proportional to $W_{\mathrm{ab}} \times W_{\mathrm{em}}$. However in the experiment, no significant chirality dependence is observed in the absorption spectra, but a chirality dependence is observed in the emission spectra, though the calculated results are opposite to the experimental results when we only consider W_{ab} and W_{em}.

Here we point out the importance of the relaxation process from E_{22}^S to E_{11}^S in determining the real PL intensity. This point is justified by the following facts : (1) only a few percent of photo-excited excitons can contribute to PL,[2] and (2) the electron-phonon interaction is much faster (0.1ps) than the photon emission process (0.1ns)[21]. Thus we need to specify which relaxation path is important for the PL process. Although the electron-phonon scattering process is restricted by the energy-momentum conservation condition of electrons and phonons, there are still many possible relaxation paths. Among them, we argue that the first step of the relaxation from E_{22}^S limits the speed of the relaxation processes, since all possible relaxation paths should start at E_{22}^S.[15] Once the electron (or hole) is relaxed from E_{22}^S, we can imagine that the exciton will be relaxed to the E_{11}^S position with some radiative relaxation probability.

In Fig. 3, we plot the relaxation rate (inverse of the relaxation time at E_{22}^S) which is given by Eq. (7), in which we consider not only phonon emission but also phonon absorption at 300K from E_{22}^S.

Because of the factor d_t in the denominator of Eq.(7), the relaxation rate is inversely proportional to d_t. Moreover the relaxation rate clearly shows a family pattern (chirality dependence) both for type I and II semiconducting SWNTs. For semiconducting SWNTs with large chiral angles (close to armchair nanotubes), the difference in $1/\tau$ between type I
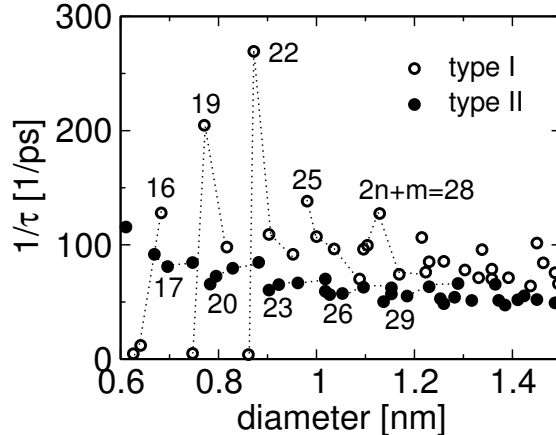
FIG. 3: The relaxation rate at E_{22}^S for semiconducting SWNTs. Open and solid dots denote type I and II semiconducting nanotubes, respectively. Points with the same indicated $2n + m$ values are connected.

and II is not so large, while for SWNTs close to the zigzag nanotube chirality, the relaxation rate for type II SWNT becomes smaller than for type I.

The strong chirality dependence and the difference between the $1/\tau$ for type I and II semiconducting tubes comes from the anisotropic electron-phonon matrix element[14] and the trigonal warping effect[20], respectively. When we consider the relaxation rate at E_{22}^S, there are two possible scattering paths: intra-valley (AV) and inter-valley (EV) scattering[15]. In EV scattering, the electron scatters from the K to K' (or from the K' to K) points in the 2D Brillouin zone, while AV scattering connects different k states near the K (or K') points, and the two processes result in different phonon wavevectors q near the K (or K') and Γ points, respectively.

The main contribution to the relaxation rate comes from LO phonons, which have energies of about 0.16eV and 0.20eV for EV and AV scattering, respectively. The related number of phonons for these energies can be calculated by using the Bose-Einstein relation for phonon emission and absorption $(\beta = 1/k_{\mathrm{B}}T)$,

$$
n_\nu(\mathbf{q}) = \begin{cases} \dfrac{1}{e^{\beta\hbar\omega_\nu(\mathbf{q})} - 1} + 1 & \text{(emission)} \\[2ex] \dfrac{1}{e^{\beta\hbar\omega_\nu(\mathbf{q})} - 1} & \text{(absorption)}. \end{cases} \tag{8}
$$

The fractional part of Eq.(8) can be neglected relative to 1 for energies larger than 0.16eV, and then we only have unity in Eq.(8) for the emission process contribution to the relaxation. For type I SWNTs, there are four (n, m) values with very small relaxation rates. That is,

9

for the (7,2), (8,0), (9,1), (11,0) tubes, the relaxation rate is almost zero, as shown in Fig. 3. This is because the energy separation between E_{22}^S and E_{11}^S is smaller than the LO phonon energy and thus there is no contribution to the relaxation from the LO phonons for these four SWNTs. The relaxation rate is a maximum for type I semiconducting SWNTs when the energy separation is close to the LO phonon energy. This maximum corresponds to (n, m) close to zigzag nanotubes such as (10,2), which like the (11,0) tube, belongs to family 22.

Though the number of acoustic phonon modes which have very small energies around the Γ point (for AV scattering) could be much larger than the number of LO phonon modes, the electron-phonon matrix elements are approximately zero for these acoustic modes. Thus, except for the LO mode, other phonon modes don't contribute much to the PL relaxation process. It should be mentioned here that we did not take into account the contribution from the acoustic phonons whose energies are smaller than 0.02eV. This is because the phonon amplitude becomes singular at finite temperature for very small phonon energies, though we know that the matrix element becomes zero from analytic expressions, and thus the overall contribution from the low energy acoustic modes can be neglected.

C. PL intensity

The PL intensity is assumed to be the product of (1) the induced photon absorption, (2) the relaxation rate at E_{22}^S and (3) the spontaneous photon emission, and the PL intensity is plotted as a function of diameter in Fig. 4. It is clear from Fig. 4 that the PL intensity is generally stronger for smaller diameter SWNTs and for type I semiconducting nanotubes, and the PL intensity exhibits an opposite chirality dependence for type I and type II tubes. The PL intensity increases (decreases) by decreasing the chiral angle for type I (II) tubes, except for the low chiral angle (7,2), (8,0), (9,1) and (11,0) type I tubes that exhibit very low PL intensities, due to their very small relaxation rates (see Section B).

D. Comparison with experiments

The (n, m) dependence for the PL intensities as calculated here can be used to understand experimental results. First of all, experimental results usually show stronger PL intensities
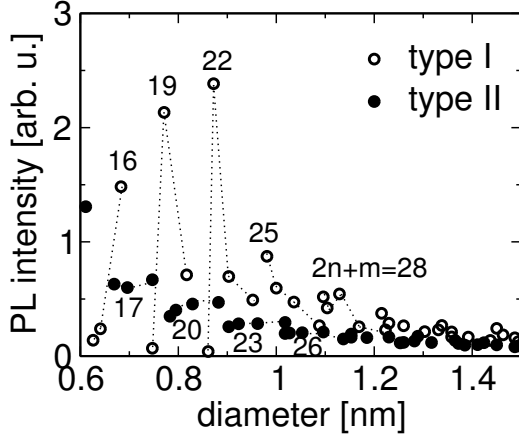
FIG. 4: PL intensity for semiconducting SWNTs. Open and solid dots are, respectively, for type I and type II semiconducting SWNTs. Points with the same indicated $2n + m$ values are connected.

for type I SWNTs[1–5]. It is unlikely that growth procedures produce more type I than type II tubes, and this intensity difference can be explained by our calculations. Another important result is the absence of PL signal from the low chiral angle (11,0) tube in HiPCO samples[2], despite the fact that this tube has a diameter ($d_t \sim 0.9$ nm) at the center of the diameter distribution in HiPCO samples ($0.6 < d_t < 1.2$ nm). Once again, it is unlikely that the (11,0) tube in particular is not produced, even if there is a preferential production of larger chiral angle tubes. The absence of PL intensity for the $(11, 0)$ tube is another result that can be explained by our calculations, providing strong support to the prediction that interband relaxation is dominated by LO phonon-related processes. It is interesting to note that a very similar type I vs type II intensity dependence was predicted by a rather different physical model (Reich *et al.*[22]), that considers exciton-exciton resonance and a constant thermalization rate. However, this excitonic model fails to predict the experimental absence of PL signal from the (11,0) tube, and overestimates the chirality dependence observed for type II tubes. In both cases the experimental results are correctly described by our calculated (n, m) dependent PL intensity calculation values.

The experimentally observed PL intensity is a product of the present calculated PL intensity for each (n, m) SWNT and the population of (n, m) SWNTs in the sample. Thus the population for each (n, m) semiconducting SWNT can be obtained by dividing the experimental PL intensity by the calculated PL intensity. The discrepancy between the calculated and experimental absorption spectra mentioned in the previous section can be
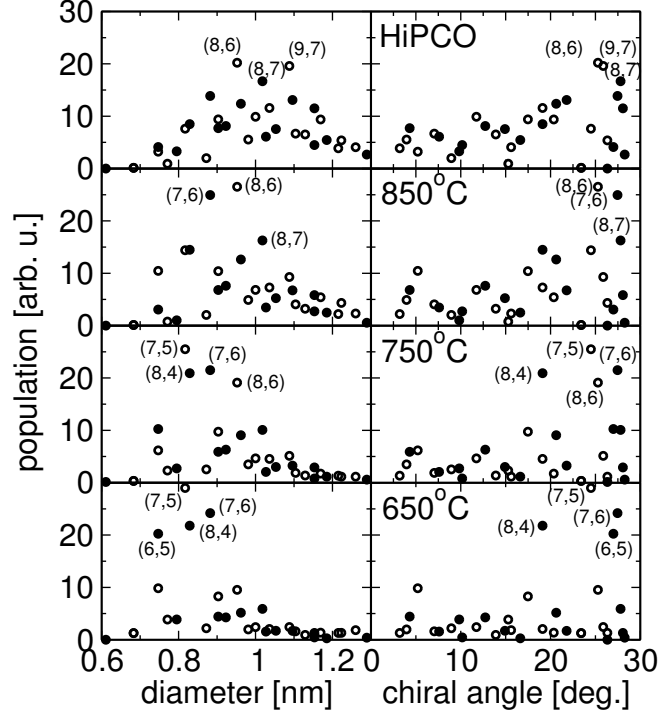
11

FIG. 5: Calculated population obtained by the ratio of the (observed PL intensity)/ (calculation PL intensity) for SWNTs prepared by the HiPCO method (at 1000°C) and by the ACCVD method at 850°C, 750°C, 650°C.

understood by some cancellation of the chirality dependence by the population effect.

In Fig. 5 we show the thus-calculated population for different samples prepared by the HiPCO method at 1000°C and for samples prepared by the (ACCVD) method[5] operating at the different temperatures of 850°C, 750°C, and 650°C. Although we see a strong chirality dependence for the calculated PL intensity, a weak chirality dependence of the population for a given diameter is observed, especially in the relatively larger diameter region. For the smaller diameter region, however, we can see a large population of SWNTs near the armchair regions. This is because the experimental results show a large PL intensity near the armchair region[5], while the calculated PL intensity gives a relatively small intensity both for type I and II semiconducting SWNTs.

In Table I, we show the calculated absorption and PL intensities for each (n, m) tube whose diameter is smaller than 1.2 nm combined with the experimental PL intensity values of HiPCO samples. This table will be convenient for the reader to understand the entries for each (n, m) value compared with Fig. 5.

It is clearly shown that the experimentally observed chirality dependence of the PL intensity comes not only from the population but comes also from the intrinsic PL dependence on chirality, except for some singularly large population of (n, m) tubes, such as the (6,5), (7,5), (7,6), (8,4), (8,6), (8,7) and (9,7) tubes which is shown in Fig. 5. The obtained population as a function of diameter (left) shows that the peak (for the dominant diameter tubes) decreases with decreasing synthesis temperature, reflecting the fact that a small cap is formed at low temperatures. An important point can be seen from the population plot as a function of chiral angle, showing some family patterns which indicate a diameter dependence for similar chiral angle SWNTs. It is pointed out that the distribution of the (n, m) population as a function of diameter is not symmetric around the peak, except for the HiPCO sample. We can see a non-uniform population in the smaller diameter region for the HiPCO tubes in Fig. 5, below the diameter where the population peaks.

We can ascribe this situation to the stability of the cap structure. In a former calculation[23], it was found that the cap of the (9,1) SWNT is about 1.0eV less stable than other caps with similar diameters, since the cap structure of the (9,1) nanotube is deformed from a hemi-spherical shape. For the (9,1) SWNT, since there is only one possible cap structure, this unstable cap is needed to grow a (9,1) SWNT. On the other hand, for a large diameter SWNT, the number of possible caps increases exponentially with increasing diameter. Thus we can find a relatively stable cap structure for small diameter tubes which should be dominant in nature. Thus even though the synthesis temperature decreases in the CVD method, the population for smaller diameter ($d_t < 0.8$nm) SWNTs is governed by the stability of the cap.

Another possible reason why the armchair nanotube is dominant in the abundance is the chirality dependence of the dispersion ability. Hashimoto *et al.* reported that near zigzag SWNTs easily form a bundle due to the stronger van der Waals force[24]. This may suggest that near armchair SWNTs have a high dispersion ability in the micellar solution.

4. SUMMARY

We have calculated the PL intensity by multiplying the photon-absorption, phonon-relaxation and photon-emission matrix elements. Photon-absorption and photon-emission matrix elements show family patterns in which the matrix elements for type I tubes are

TABLE I: Calculated absorption and PL intensities and experimental PL intensities for a HIPCO sample for each (n, m) tube whose diameter is smaller than 1.2 nm in arbitrary units. The left and right sides correspond to SWNTs of type I and type II, respectively.

		type I						type II			
(n,m)	d_t [nm]	θ [°]	W_{ab}	I_{PL}	I_{HiPCO}	(n,m)	d_t [nm]	θ [°]	W_{ab}	I_{PL}	I_{HiPCO}
(6,4)	0.69	23.49	2.16	1.48	0.14	(6,5)	0.75	27.02	1.85	0.67	4.12
(7,5)	0.82	24.54	2.04	0.71	7.61	(7,6)	0.89	27.47	1.98	0.47	13.86
(8,3)	0.78	15.40	2.43	2.13	0.93	(8,4)	0.83	19.19	1.77	0.46	8.49
(8,6)	0.96	25.31	2.18	0.49	20.20	(8,7)	1.02	27.80	2.06	0.30	16.68
(9,1)	0.75	5.40	2.75	0.07	3.22	(9,2)	0.80	9.95	1.67	0.40	3.29
(9,4)	0.91	17.53	2.27	0.70	9.39	(9,5)	0.97	20.66	1.88	0.28	12.38
(9,7)	1.09	25.88	2.22	0.27	19.59	(9,8)	1.16	28.06	2.14	0.19	11.51
(10,2)	0.88	9.09	2.67	2.38	1.99	(10,3)	0.93	12.79	1.80	0.28	8.13
(10,5)	1.04	19.16	2.33	0.47	11.58	(10,6)	1.10	21.81	2.03	0.21	13.09
(11,3)	1.00	11.79	2.53	0.59	9.90	(11,1)	0.91	4.41	1.73	0.26	7.72
(11,6)	1.17	20.37	2.42	0.26	9.38	(11,4)	1.06	14.95	1.93	0.20	7.54
(12,1)	0.98	4.04	2.63	0.87	5.53	(12,2)	1.03	7.67	1.87	0.20	6.08
(12,4)	1.13	13.97	2.57	0.54	6.52	(12,5)	1.19	16.64	2.13	0.16	5.44
(13,2)	1.11	7.09	2.52	0.42	6.67	(13,3)	1.15	10.18	1.98	0.17	4.49

larger than for type II because of the trigonal warping effect of the electronic structure and because for near zigzag SWNTs a larger (smaller) matrix element is predicted than for near armchair SWNTs for type I (type II) semiconducting SWNTs. The relaxation rate at E_{22}^S shows that the optic LO phonon gives a large contribution to the relaxation rate. When the energy separation between E_{22}^S and E_{11}^S is smaller than the LO phonon mode energy, the rate drastically decreases and suppresses the PL intensity. By dividing the experimental PL intensity by the calculated PL intensity, we get the population of individual (n, m) SWNTs for different synthesis temperatures. The peak tube diameter shifts to a larger diameter with increasing synthesis temperature. For smaller nanotubes, we found that some (n, m) SWNTs with chiral angles near armchair SWNTs gives a large population among the SWNTs, and this effect may be related to their stable cap structure.

5. ACKNOWLEDGMENTS

6. REFERENCES

[1] O'Connell MJ, Bachilo SM, Huffman XB, Moore VC, Strano MS, Haroz EH, et al. Band gap fluorescence from individual single walled carbon nanotubes. Science 2002;297:593-6.

[2] Bachilo SM, Strano MS, Kittrell C, Hauge RH, Smalley RE, Weisman RB. Structure-assigned optical spectra of single walled carbon nanotubes. Science 2002;298:2361-6.

[3] Strano MS. Probing Chiral Selective Reactions Using a Revised Kataura Plot for the Interpretation of Single-Walled Carbon Nanotube Spectroscopy. J Am Chem Soc 2003;125:16148-53.

[4] Strano MS, Zheng M, Jagota A, Onoa GB, Heller DA, Barone PW. Understanding the Nature of the DNA-Assisted Separation of Single-Walled Carbon Nanotubes Using Fluorescence and Raman Spectroscopy. Nano Letters 2004;4:543-50.

[5] Miyauchi Y, Chiashi S, Murakami Y, Hayashida Y, Maruyama S. Fluorescence spectroscopy of single-walled carbon nanotubes synthesized from alcohol. Chem Phys Lett 2004;387:198-203.

[6] Samsonidze GG, Saito R, Kobayashi N, Grüneis A, Jiang J, Jorio A, et al. Family behavior of the optical transition energies in single-wall carbon nanotubes of smaller diameters. Appl Phys Lett 2004;85:5703-5.

[7] Jorio A, Fantini C, Pimenta MA, Capaz RB, Samsonidze GG, Dresselhaus G, et al. Resonance Raman spectroscopy (n,m)-dependent effects in small-diameter single-wall carbon nanotubes. Phys Rev B 2005;71:075401.

[8] Jiang J, Saito R, Grüneis A, Chou SG, Samsonidze GG, Jorio A, et al. Intensity of the resonance Raman excitation spectra of single-wall carbon nanotubes. Phys Rev B 2005;71:205420.

[9] Jiang J, Saito R, Grüneis A, Dresselhaus G, Dresselhaus MS. Electron-phonon interaction and

relaxation time in graphite. Chem Phys Lett 2004;392:383-9.

[10] Grüneis A, Saito R, Samsonidze GG, Kimura T, Pimenta MA, Jorio A, et al. Inhomogeneous optical absorption around the K point in graphite and carbon nanotubes. Phys Rev B 2003;67:165402.

[11] Ajiki H, Ando T. Aharonov-Bohm effect in carbon nanotubes. Physica B Condensed Matter 1994;201:349-52.

[12] Schiff LI. Quantum Mechanics. McGraw-Hill: Singapore. 1968:530-3

[13] Porezag D, Frauenheim Th, Köhler Th, Seifert G, Kaschner R. Construction of tight-binding-like potentials on the basis of density-functional theory: Application to carbon. Phys Rev B 1995;51:12947-57.

[14] Jiang J, Saito R, Samsonidze GG, Chou SG, Jorio A, Dresselhaus G, et al. (submitted).

[15] Jiang J, Saito R, Grüneis A, Chou SG, Samsonidze GG, Jorio A, et al. Photoexcited electron relaxation processes in single-wall carbon nanotubes. Phys Rev B 2005;71:045417.

[16] Ando T. Excitons in Carbon Nanotubes. J Phys Soc Jpn 1997;66:1066-73.

[17] Spataru CD, Ismail-Beiqi S, Benedict LX, Louie SG. Excitonic Effects and Optical Spectra of Single-Walled Carbon Nanotubes. Phys Rev Lett 2004;92:077402.

[18] Perebeinos V, Tersoff J, Avouris Ph. Scaling of Excitons in Carbon Nanotubes. Phys Rev Lett 2004;92:257402.

[19] Jorio A, Santos AP, Ribeiro HB, Fantini C, Souza M, Vieira JPM, et al. Quantifying carbon-nanotube species with resonance Raman scattering. Phys Rev B 2005;72:075207.

[20] Saito R, Dresselhaus G, Dresselhaus MS. Trigonal warping effect of carbon nanotubes. Phys Rev B 2000;61:2981-90.

[21] Klingshirn CF, Semiconductor Optics. Springer: Berlin. 2004.

[22] Reich S, Thomsen C, Robertson J. Exciton Resonances Quench the Photoluminescence of Zigzag Carbon Nanotubes. Phys Rev Lett 2005;95:077402.

[23] Maruyama S, et al. (private communication).

[24] Hashimoto A, Suenaga K, Urita K, Shimada T, Sugai T, Bandow S, et al. Atomic Correlation Between Adjacent Graphene Layers in Double-Wall Carbon Nanotubes. Phys Rev Lett 2005;94:045504.